**Showcasing the research from Lili Hu's research group, Key Laboratory of Materials for High Power Laser, Shanghai Institute of Optics and Fine Mechanics, Chinese Academy of Sciences.**

Broadband L+ near-infrared luminescence in bismuth/germanium co-doped silica glass prepared by the sol–gel method

Bismuth (Bi) and germanium (Ge) co-doped silica glass and fiber exhibit L+ near-infrared (NIR) luminescence, contributing to the broadening of communication band. We prepared Bi/Ge co-doped silica glass by a sol–gel method and elucidated the behavior of bismuth NIR luminescence, revealing a direct correlation between BAC-Ge responsible for L+ band emission and Ge-ODC. This study serves as a valuable reference for the design of bismuth-doped silica fiber for L+ band amplification applications.
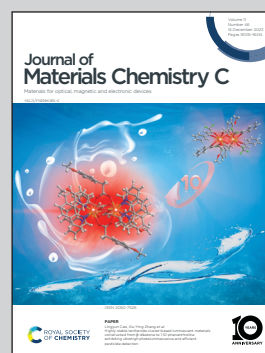
ROYAL SOCIETY
OF **CHEMISTRY**

rsc.li/materials-c

PAPER

Check for updates

Broadband L+ near-infrared luminescence in bismuth/germanium co-doped silica glass prepared by the sol–gel method

Xin Li, [ID] [ab] Mengting Guo, [a] Chongyun Shao, [a] Jinming Tian, [a] Fan Wang, [a] Yinggang Chen, [ab] Yan Jiao, [a] Chunlei Yu*[ac] and Lili Hu*[ac]

Bismuth (Bi) and germanium (Ge) co-doped silica glass and fiber, as novel amplification media, have attracted extensive attention due to their L+ near-infrared (NIR) luminescence to broaden the communication band. However, the underlying mechanism of bismuth NIR luminescence remains elusive, which poses a constraint on the development of Bi/Ge co-doped silica glass and fiber. In this study, Bi/Ge co-doped silica glass was prepared by a sol–gel method and the influence of Ge and Bi doping concentrations on luminescence properties was systematically investigated. Through an analysis of the glass network structure, a direct correlation between bismuth near-infrared active luminescence centers (BAC) for L+ band emission and the germanium oxygen vacancy defects (Ge-ODC) was found. The formation mechanism of BAC-Ge was proposed. This paper provides insights into bismuth NIR luminescence behavior, especially in the L+ band and serves as a valuable reference for the precise design of bismuth-doped silica fiber for L+ band amplifying applications.

1. Introduction

In the current communication system, the demand for high-speed transmission capacity in optical communication is rapidly escalating. At present, rare-earth (RE) doped silica glass and fiber serve as extensively employed gain media for optical amplifiers and tunable fiber lasers.[1–3] Among them, erbium (Er)-doped fiber finds extensive utilization within communication systems.[4,5] However, Er^{3+} has narrow band luminescence, which cannot meet the need for widening the communication band. Finding a new type of optical material with broadband near-infrared (NIR) emission is urgently needed. Bismuth (Bi) doped materials have attracted widespread attention because of their broadband NIR luminescence covering the O, E, S, C, L and L+ communication bands by adjusting their composition and preparation process.[6–12] Therefore, Bi-doped fibers are considered promising candidates in the tunable fiber lasers and broadband amplifiers.[13–16]

In previous studies, researchers have successfully achieved optical amplification in the wavelength ranges of 1350–1500 nm

and 1600–1800 nm by co-doped germanium and bismuth in silica fibers.[17–20] This advancement holds significance for expanding communication bandwidth through integration with Er^{3+} L-band amplification.[20–22] The consensus attributes the luminescence observed within these spectral bands to bismuth near-infrared active luminescence centers (BAC), which have been named BAC-Si and BAC-Ge for the respective wavelength range.[19,20] Numerous research studies have mainly focused on optical amplification and laser phenomena of Bi-doped silica fiber, or the influence of various factors on them.[18,23,24]

Concurrently, significant research efforts have been dedicated to germanium-doped silica glass and fiber. A large number of studies explored their glass network structure, optical properties and defects.[25–28] This creates an advantageous condition for investigating the relationship between BAC and the glass structure. Speculation has arisen regarding a potential close connection between BAC and germanium defects, particularly germanium oxygen vacancy defects (Ge-ODC).[29,30] However, a deficiency of direct evidence has hindered the elucidation of the formation mechanism of BAC, particularly in terms of its connection with germanium defects. For the widespread potential application of Bi/Ge co-doped silica materials, exploring the mechanism of Bi NIR luminescence is necessary.

In this paper, we prepared Bi/Ge co-doped silica glass by the sol–gel method combined with a high temperature sintering method.[31] Notably, this marks the first instance of successfully preparing this glass composition. The optical properties and

[a] Key Laboratory of Materials for High Power Laser, Shanghai Institute of Optics and Fine Mechanics, Chinese Academy of Sciences, Shanghai 201800, People's Republic of China. E-mail: sdycllcy@163.com, hulili@siom.ac.cn

[b] Center of Materials Science and Optoelectronics Engineering, University of Chinese Academy of Sciences, Beijing 100049, People's Republic of China

[c] Hangzhou Institute for Advanced Study, University of Chinese Academy of Sciences, Hangzhou 310024, People's Republic of China

16152 | *J. Mater. Chem. C*, 2023, **11**, 16152–16158

This journal is © The Royal Society of Chemistry 2023

structures of the homogeneous bulk glass sample were characterized. Additionally, the oxygen-deficient preparation conditions induced a substantial concentration of Ge-ODC within the glass network, which has a direct correlation with BAC-Ge. In detail, we investigated the effect of germanium and bismuth doping concentration on BAC-Ge NIR luminescence. Furthermore, we analyzed the structure of the glass network and proposed a plausible mechanism for the formation of BAC-Ge.

2. Experimental procedure

2.1 Sample preparation

Two series of glass samples with nominal compositions of $(99.99 - x)SiO_2-xGeO_2-0.01Bi_2O_3$ (x = 20, 30, 40, 50, and 60 mol%; named xGe) and $(50 - 0.01y)SiO_2-50GeO_2-0.01yBi_2O_3$ (y = 0, 1, 2, 4, 6, and 10 mol%; named yBi) were prepared by the sol–gel method combined with high temperature sintering in a vacuum tungsten wire furnace. The detailed preparation process has been described in our previous work.[31] 99.99% tetraethoxysilane, C_2H_5OH, $GeCl_4$ and $BiCl_3\cdot6H_2O$ were used as starting materials, whereas ethanol was used as the solvent, and de-ionized water was introduced to maintain the hydrolysis reaction. All samples were polished optically for further characterization. The refractive index and actual content (tested by ICP-AES) of the xGe samples are shown in Table 1. Each mole of germanium oxide causes a 0.0014 refractive index increase of glass.

2.2 Sample characterization

Optical transmittance spectra were recorded using a PerkinElmer Lambda 900 Ultraviolet-Visible-Near-infrared (UV-Vis-NIR) spectrophotometer over the spectral range from 190 to 1600 nm. Static excitation and emission spectra as well as emission lifetimes were obtained using an Edinburgh FLS920 spectrofluorometer equipped with a continuous wave 150 mW Xe lamp, an 808 nm/915 nm laser diode (LD) and a microsecond flashlamp (μF900) as excitation sources.

Fourier transform infrared (FTIR) spectra were obtained using a Nicolet 6700 spectrophotometer (Bruker, Germany) by dispersing glass powders into KBr pellets. The Raman spectra in the range of 200–1500 cm^{-1} were recorded using a Horiba LabRAM HR Evolution Raman microscope with a 633 nm laser as the excitation source. The CW-EPR measurements of the paramagnetic point defects were conducted employing a BRUKE ELEXSYS-II E500 CW-EPR spectrometer operating in the X-band (9.85 GHz) with a microwave power of 1 mW in the 350–360 mT magnetic field range. The CW-EPR spectra were normalized to the same receiver gain and a sample weight of 1 mg. All the above measurements were carried out at room temperature.

3. Results and discussion

3.1 Optical properties of Bi NIR luminescence

Fig. 1 presents the absorption spectra of xGe samples and yBi samples, and the inset shows the photographs of the yBi glass samples. Fig. 1(a) reveals two absorption peaks positioned at 420 nm and 463 nm, corresponding to BAC-Si and BAC-Ge within the Ge/Bi co-doped silica glass, respectively.[19] With the addition of germanium, the absorption intensity of BAC-Si gradually decreased, eventually disappearing in the 40Ge sample. Conversely, the amount of BAC-Ge gradually increased and reached a maximum in the 50Ge sample. In Fig. 1(b), the absorption coefficient gradually increased as the Bi content increased from 0.01 to 0.1 mol%. The same result is manifested in the color of the glass sample as shown in the inset, which changed from light to dark with the addition of Bi_2O_3 content. Here, we infer that it is due to intense absorption of bismuth clusters in the visible region.

According to the report of Dianov,[32] BAC-Si exhibits an absorption band centered at $\sim$820 nm, while BAC-Ge exhibits an absorption band at $\sim$920 nm. Because of the broad absorption characteristics of bismuth ions, BAC-Si and BAC-Ge can be effectively excited by 808 nm and 915 nm as depicted in Fig. 2(a–d). Under 808 nm excitation, all samples exhibit a primary peak at 1400 nm attributed to BAC-Si and a shoulder peak at 1650 nm attributed to BAC-Ge. However, it is worth noting that a study in ref. 19 suggests that BAC-Ge does not exhibit an absorption peak at approximately 808 nm.[19] Therefore, it is reasonable to infer that there is an energy transfer process from BAC-Si to BAC-Ge under 808 nm excitation. A Gaussian peak fitting approach was used to analyze the emission spectrum of the 50Ge sample, as depicted in Fig. 2(e). The peak position of BAC-Si is at $\sim$1380 nm and that of BAC-Ge is at $\sim$1620 nm. Additionally, the peak area ratios of BAC-Si and BAC-Ge were calculated for all samples, and the results are presented in Fig. 2(f) and (g). In contrast, under 915 nm excitation, there is only one peak at 1680 nm in all samples, ascribed to BAC-Ge.

Table 1 The refractive index and actual content of the xGe samples

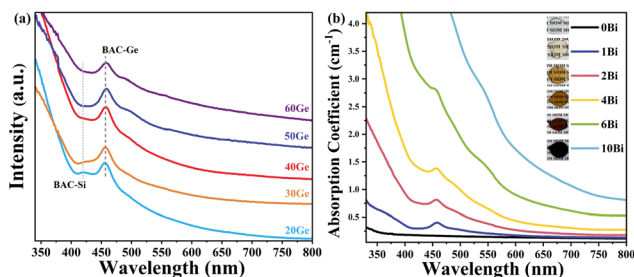| Glass	Refractive index		GeO$_2$ content (wt%)	Bi content (wt%)
	@633	@1064		
20Ge	1.48216	1.47388	26.21	0.12
30Ge	1.49248	1.48656	38.23	0.13
40Ge	1.50660	1.49782	47.17	0.13
50Ge	1.52013	1.51109	58.35	0.13
60Ge	1.53149	1.52341	66.02	0.14

Fig. 1 The absorption spectra of (a) xGe samples and (b) yBi samples. The inset is the photographs of glass samples. The sample thickness is 1 mm.
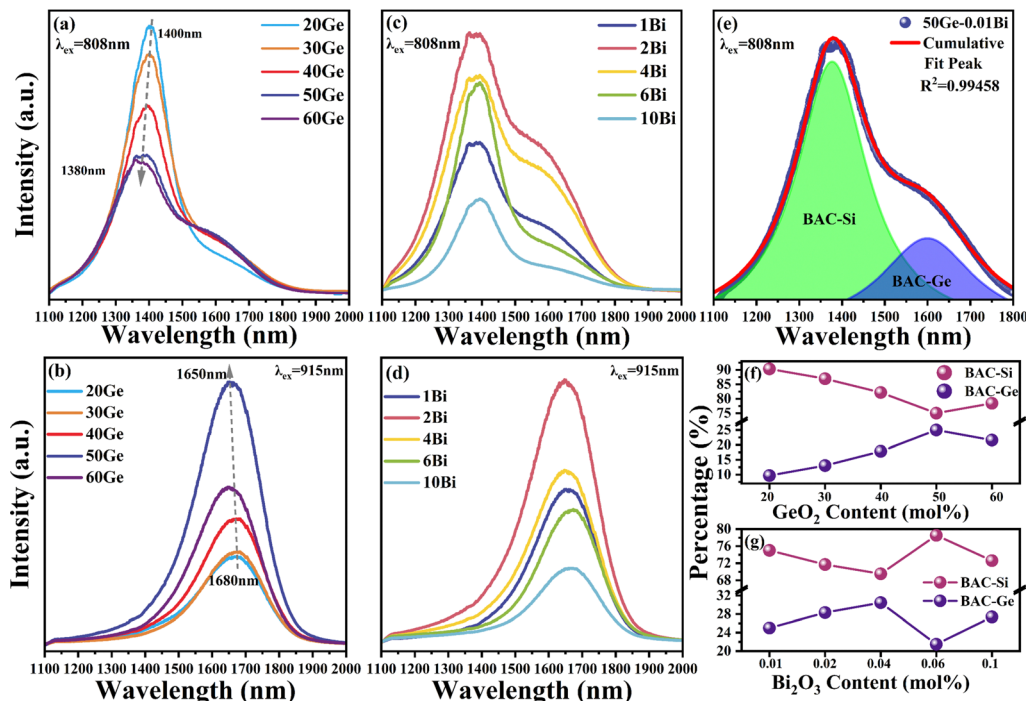
Fig. 2 Emission spectra of xGe samples excited at (a) 808 nm and (b) 915 nm and yBi samples excited at (c) 808 nm and (d) 915 nm. (e) Gaussian multipeak fit of the emission spectrum of 50Ge samples excited at 808 nm. The peak area ratios of BAC-Si and BAC-Ge excited at 808 nm in different (f) GeO$_2$ and (g) Bi$_2$O$_3$ contents.

As shown in Fig. 2(a) and (b), the content of GeO$_2$ can significantly affect the emission intensity and peak position of bismuth ions in glass. When the GeO$_2$ content increased, the intensity at 1400 nm decreased, whereas that at 1680 nm enhanced. In Fig. 2(f), the peak area ratios of BAC-Si and BAC-Ge exhibit analogous changes excited at 808 nm. There may be a transformation of bismuth active centers from BAC-Si to BAC-Ge with the substitution of GeO$_2$ for SiO$_2$. When the GeO$_2$ concentration reached 50 mol%, the BAC-Ge content achieved a maximum. In the 60Ge sample, the fluorescence intensity is weaker than 50Ge, indicating the smaller amount of BAC-Ge in the 60Ge sample. In addition, the emission peak of BAC-Si is blue shifted from 1400 to 1380 nm, and that of BAC-Ge simultaneously is blue shifted from 1680 to 1650 nm with the increase of GeO$_2$. This phenomenon may be related to the increment of field strength around Bi ions.[9]

Fig. 2(c) and (d) show the influence of the Bi content on the emission spectra with a fixed GeO$_2$ content of 50 mol%. Upon introducing Bi, the intensity of NIR luminescence is initially amplified, followed by a subsequent decline attributed to the formation of bismuth clusters. That is, the optimal Bi$_2$O$_3$ content is 0.02 mol%. When the Bi$_2$O$_3$ content is > 0.06 mol%, Bi NIR luminescence is quenched by bismuth clusters. Comparing the emission peak areas of BAC-Si and BAC-Ge excited at 808 nm (Fig. 2(g)), it becomes evident that bismuth clusters exert a more pronounced influence on BAC-Ge. This result is in agreement with the sample color; as the number of bismuth clusters increases, the absorption of the visible band increases, and it leads the color of the sample turning black.
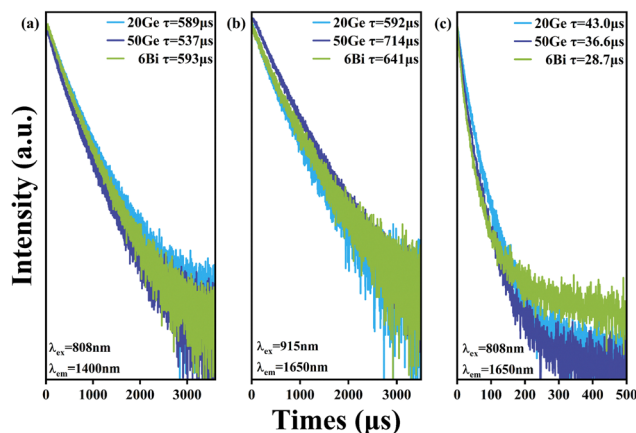

Fig. 3 Photoluminescence decay spectra of 20Ge, 50Ge and 6Bi samples: (a) 1400 nm excited by 808 nm, (b) 1650 nm excited by 915 nm, and (c) 1650 nm excited by 808 nm.

To distinguish the bismuth active center, we selected 20Ge, 50Ge and 6Bi samples as representatives to measure the photoluminescence decay spectra. Fig. 3 shows the decay curves with emissions at 1400 nm and 1650 nm under excitations of 808 nm and 915 nm. Both bismuth active centers, BAC-Si and BAC-Ge, have double exponential lifetimes, which means that each luminescence is attributed to at least two kinds of luminescence centers.[33] This phenomenon might arise from variations in the bismuth ion coordination environment in glass. Here, we used average fluorescence lifetime $\bar{\tau}$ to characterize the coordination environment around the BAC.[10,33]

16154 | J. Mater. Chem. C, 2023, 11, 16152–16158

This journal is © The Royal Society of Chemistry 2023

The average fluorescence lifetime $\bar{\tau}$ can be evaluated using the following equation:[34]

$$\bar{\tau} = \int I(t)t\,\mathrm{d}t \Big/ \int I(t)\mathrm{d}t \tag{1}$$

where $I(t)$ represents the fluorescence intensity I at time t. The average fluorescence lifetime $\bar{\tau}$ is marked in Fig. 3.

A comparative analysis of the fluorescence lifetimes between the 20Ge and 50Ge samples is made to elucidate the impact of GeO_2 content, and the same analysis is done on the fluorescence lifetimes of the 50Ge and 6Bi samples to elucidate the impact of the Bi_2O_3 content. With the addition of GeO_2, the fluorescence lifetime at 1400 nm excited by 808 nm, corresponding to the BAC-Si, was shortened. However, the fluorescence lifetime at 1650 nm excited by 915 nm, corresponding to the BAC-Ge, was prolonged. The fluorescence lifetime at 1650 nm excited by 808 nm in Fig. 3(c) is an order of magnitude shorter than those of BAC-Si and BAC-Ge by 915 nm excitation in Fig. 3(a) and (b), indicating that this process is not directly excited BAC-Ge at 808 nm excitation, and the energy transfer from BAC-Si to BAC-Ge occurred.

Comparing the fluorescence lifetimes of 50Ge and 6Bi samples, it is seen that with the increase of Bi_2O_3, the fluorescence lifetime of BAC-Si increased due to an increase in the amount of BAC-Si as shown in Fig. 3(a). In contrast, the fluorescence lifetime of BAC-Ge decreases with the increase of bismuth as shown in Fig. 3(b). This decrease in the fluorescence lifetime of BAC-Ge is attributed to the aggregation of bismuth ions into clusters, which absorb energy from BAC-Ge. Due to non-radiative energy transfer processes, this aggregation causes the shortening of fluorescence lifetime of BAC-Ge. This further illustrates that in the glass matrix of 50Ge–50Si, Bi clusters primarily affect BAC-Ge, possibly due to their preference for gathering around germanium atoms within the glass network, influenced by the germanium coordination environment. Similarly, the shortened fluorescence lifetime of the 1650 nm emission, when excited at 808 nm, can also be attributed to the increase in Bi clusters.

3.2 Spectroscopic properties of BAC-Ge and Ge-ODC

To further understand the spectral properties of Bi/Ge co-doped silica glass, a visible excitation mapping spectrum of the 50Ge sample was obtained and is illustrated in Fig. 4. It is known from Fig. 4 that broadband luminescence of bismuth ions at 1680 nm can be excited by 380 nm and 460 nm. Notably, apart from the reported excitation wavelength of 463 nm,[19] a previously undefined excitation peak emerges at 380 nm. Under the excitation at 380 nm, the luminescence of BAC-Si is much weaker. The previous reports speculated that the UV absorption of bismuth is related to the oxygen vacancy defects in the glass network.[35] Considering that all samples are prepared in the vacuum tungsten furnace, there must be germanium oxygen vacancy defects (Ge-ODC) in the glass network which luminesces at $\sim$380 nm.[28] A potential connection between Ge-ODC and BAC-Ge warrants further exploration.
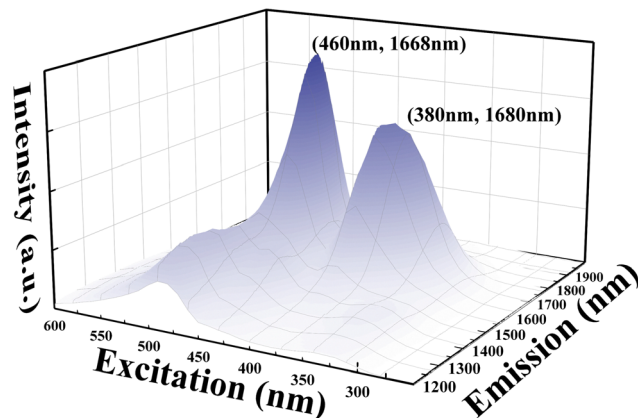

Fig. 4 Three-dimensional excitation–emission of the 50Ge sample.

To verify the above assumption, we characterized the optical properties of Ge-ODC, as shown in Fig. 5. Under the excitation at 258 nm (Fig. 5(a) and (b)), all the samples have two luminescence peaks, *i.e.*, a weak emission peak at 300 nm due to the singlet–singlet transition and a strong emission peak at 400 nm due to the triplet–singlet transition of Ge-ODC.[28] Furthermore, it is important to note that the absorption properties of Si-ODC differ significantly, with an absorption located at 5.0 eV and fluorescence at 2.7 eV and 4.3 eV.[36] In addition, previous studies showed that Ge–Ge vacancy has a lower formation energy than Si–Si vacancy.[37,38] Given these distinctions, we posit that the number of Si-ODC is ignorable in the glass network.

In Fig. 5(a), the emission intensity of Ge-ODC decreases with the increasing GeO_2 content, and the minimum is for the 50Ge sample. Interestingly, this trend is inversely proportional to the NIR luminescence intensity of BAC-Ge as shown in Fig. 2(b). In Fig. 5(b), it is obvious that the increase of the Bi_2O_3 content substantially reduces the fluorescence intensity of Ge-ODC, which means that the energy transfer from Ge-ODC to BAC-
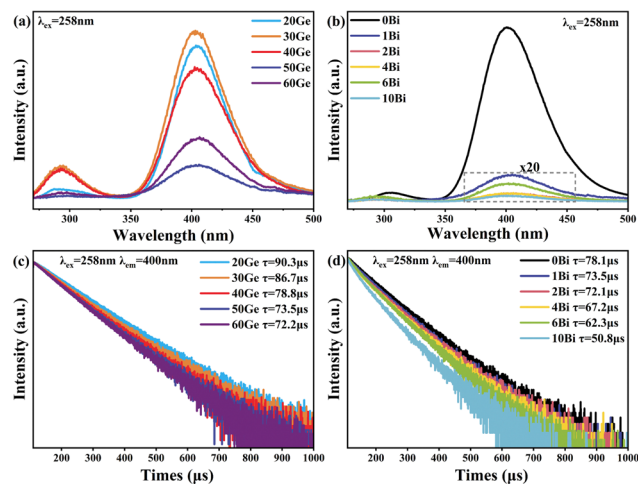

Fig. 5 Emission spectra excited by 258 nm of (a) xGe samples and (b) yBi samples. Photoluminescence decay spectra of 400 nm excited by 258 nm of (c) xGe samples and (d) yBi samples.

This journal is © The Royal Society of Chemistry 2023

J. Mater. Chem. C, 2023, **11**, 16152–16158 | **16155**

Ge happened. As Essid *et al.* reported, the Ge-ODC defects increase with the increase of the GeO_2 content in silica.[39] Therefore, the increase in the number of BAC-Ge results in a reduction in the fluorescence of Ge-ODC. Additional insights are gained through the decay spectrum of Ge-ODC, as presented in Fig. 5(c) and (d). All the samples show single exponential decay, which means that the luminescence behavior is ascribed to Ge-ODC. The decay can be fitted by the following eqn (2), and the lifetime τ is shown in Fig. 5(c) and (d).

$$I(t) = I_0 \exp(-t/\tau) \tag{2}$$

The fluorescence lifetime τ decreased with the increasing GeO_2 content. Furthermore, the lifetime decreased with the addition of the Bi_2O_3 content, indicating that bismuth ions play a significant role in influencing Ge-ODC behavior. Specifically, it generates an energy transfer process from Ge-ODC to BAC-Ge, which leads to a reduction in the fluorescence lifetime of Ge-ODC.

In previous research, the relationship between Ge-ODC and BAC-Ge was not clear due to the lack of detailed characterization.[19] Here, we believe that the excitation peak at 380 nm belongs to BAC-Ge, and there is an energy transfer between Ge-ODC and BAC-Ge. The simplified energy level diagrams of Ge-ODC and BAC-Ge are shown in Fig. 6. In this scheme, Ge-ODC absorbs energy at 258 nm, transmitting to the S1 and S2 energy levels, followed by an intersystem crossing (ISC) process to reach the T1 energy level.[28] Subsequently, an energy transfer transpires to the ES$_4$ level of BAC-Ge, thereby giving rise to the near-infrared luminescence observed at 1680 nm.

3.3 Structures of Bi/Ge co-doped silica glasses

In the previous sections, we characterized the optical properties of the Bi/Ge co-doped silica glass. Owing to the outermost 6s6p electronic structure of the bismuth ion, its NIR lumines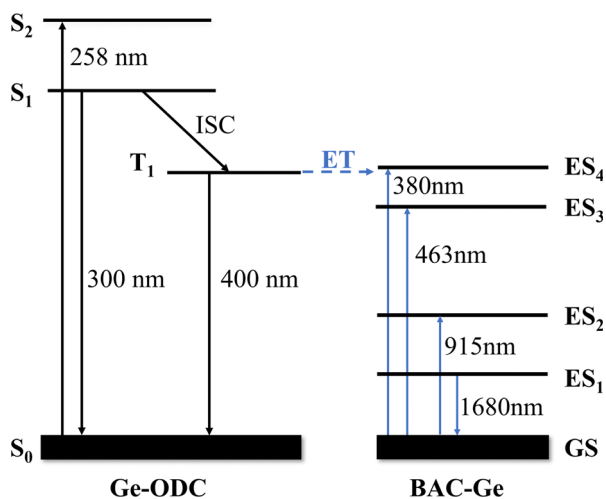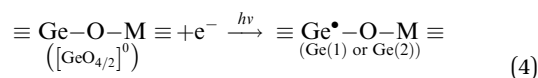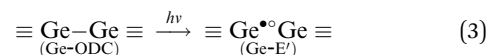cence behavior is sensitive to the encompassing coordination environment.[40] In order to further investigate the factors influencing the Bi NIR luminescence, we measured the FTIR, Raman and electron paramagnetic resonance (EPR) spectra of glasses to illustrate the surrounding coordination environment around the bismuth active center.

Because of the low doping concentration of Bi ions (<0.1 mol%) in the glasses, there is a negligible effect on the structure of the glass network. Consequently, we subjected the *x*Ge sample to characterization using FTIR and Raman spectra, as depicted in Fig. 7(a) and (b). With combined analysis of Raman and FTIR spectra, the Si–O–Si, Si–O–Ge and Ge–O–Ge bonds in the glass network can be observed,[25,41,42] and the attribution of the individual peaks is shown in Table 2. With the increase of GeO_2, the intensity of the peaks at 465 and 800 cm^{-1} of FTIR and the peaks at 438, 800 and 1054 cm^{-1} of Raman spectra reduced. Conversely, the intensity of the peaks at 680 and 880 cm^{-1} of FTIR and the peaks at 525–600 cm^{-1} of Raman spectra enhanced. These observations imply the replacement of the part of the Si–O–Si band by the Ge–O–Ge band, thereby inducing changes in the coordination environment surrounding bismuth. In essence, the transformation from BAC-Si to BAC-Ge is implied.

To obtain details of the glass network, especially about the Ge-ODC, we use EPR to analyze. However, Ge-ODC is an anti-magnetic defect and cannot be directly characterized by CW-EPR. As shown in Fig. 8(a), all the samples have no CW-EPR signals about Si or Ge defects. Here, we irradiated all samples with 1 kGy γ-ray to obtain Ge-related defects which can be detected by CW-EPR. According to our previous reports, a 1 kGy irradiation dose can produce the defects related to Ge, the defect in the sample after irradiation had changed as follows.[43]

$$\underset{(Ge\text{-}ODC)}{\equiv Ge\text{-}Ge \equiv} \xrightarrow{h\nu} \underset{(Ge\text{-}E')}{\equiv Ge^{\bullet\circ}Ge \equiv} \tag{3}$$

$$\underset{([GeO_{4/2}]^0)}{\equiv Ge\text{-}O\text{-}M \equiv + e^-} \xrightarrow{h\nu} \underset{(Ge(1)\text{ or }Ge(2))}{\equiv Ge^{\bullet}\text{-}O\text{-}M \equiv} \tag{4}$$

$$(M = Si \text{ or } Ge)$$

where M refers to the next nearest neighbor positions of the Ge atom. The Ge(1) defect will be generated by irradiation when the next nearest neighbor atom around the $[GeO_{4/2}]^0$ group is a Si atom. Conversely, when the next nearest neighbor atom is the Ge atom, it will produce the Ge(2) defect. The defects
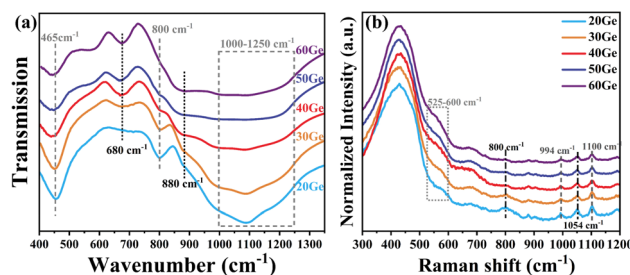

Fig. 6 Simplified energy level diagrams of Ge-ODC and BAC-Ge. The possible energy transfer processes are indicated by blue dashed lines.

Fig. 7 (a) FTIR spectra and (b) Raman spectra of *x*Ge samples.

16156 | *J. Mater. Chem. C*, 2023, **11**, 16152–16158

This journal is © The Royal Society of Chemistry 2023

Table 2 The attribution of Raman and FTIR peaks in Ge-doped silica glass

FTIR wavenumber (cm^{-1})	Raman shift (cm^{-1})	Assignment
465, 800	438, 800, 1054	Si–O–Si
680	—	Vibrations of Ge–O$^-$ in GeO$_6$ units
880	525–600	Ge–O–Ge
1000–1250	994, 1100	Si–O–Ge

Fig. 9 Schematic representation of the Bi/Ge co-doped silica glass network.

Fig. 8 CW-EPR spectra of xGe samples (a) without irradiation and (b) after 1 kGy γ-ray irradiation. (c) Splitting peaks of the 20Ge sample. (d) Percentages of various paramagnetic defects.

of Ge-E′, Ge(1) and Ge(2) can be characterized by CW-EPR,[26] and the result is shown in Fig. 8(b).

The CW-EPR spectra revealed a composited structure of Ge-E′, Ge(1) and Ge(2) from 351 to 355 mT.[26] According to splitting peaks by SpinCount software and calculating the area of the double integral, the peak splitting result of the 20Ge–0.01Bi sample is illustrated in Fig. 8(c), while the proportions of each defect are depicted in Fig. 8(d). With the increase of the GeO$_2$ content the proportion of Ge(1) increased and the Ge(2) decreased, which means that the Ge–O–Si band is more susceptible to breakage. The percentage of Ge-E′ elevated with the augmentation of the germanium concentration, reaching the maximum for the 50Ge sample. According to eqn (3), Ge-ODC serves as the precursor for Ge-E′, suggesting that the 50Ge sample contains the highest concentration of Ge-ODC. However, Fig. 5(a) shows that the 50Ge sample exhibits the lowest fluorescence intensity of Ge-ODC, implying the most efficient energy transfer from Ge-ODC to BAC-Ge happened in this sample. From this perspective, a large number of Ge-ODC defects result in the generation of more BAC-Ge.

Combining the result of the emission spectra and the EPR spectra, it is obvious that the formation of BAC-Ge has a direct

relationship with the Ge-ODC. In this context, we propose a plausible formation mechanism of BAC-Ge from the aspect of charge balance. Current research suggested that the origin of bismuth near-infrared luminescence is from low-valent bismuth ions.[44] As X. Li *et al.* reported, Bi ions will change to low-valent when the valence state of the coordination environment increased.[33] This can illustrate the relationship between Ge-ODC and BAC-Ge, and the possible schematic representation of the Bi ions in the Ge/Si silica glass network is shown in Fig. 9. During the glass melting process previously described, the lack-oxygen environment leads to the formation of Ge-ODC in the glass network which is confirmed by Fig. 5(a). In an effort to equilibrate electric charge, the high valence state environment around Ge-ODC prompts a transition of Bi ions to a low-valence state. Consequently, the presence of low-valent Bi ions, serving as active luminescence centers (BAC), becomes concentrated around Ge-ODC.

4. Conclusions

In summary, we studied the effect of bismuth ion and germanium oxide concentrations on the NIR luminescence behavior of Bi/Ge co-doped silica glass in detail. Glasses were prepared by the sol–gel method combined with high-temperature sintering. We systematically explored the relationship between spectroscopic properties and glass structures, employing analytical techniques encompassing absorption, emission, FTIR, Raman, and EPR spectroscopies. The findings demonstrate that increasing the concentration of germanium oxide leads to the enhancement of L+ band fluorescence intensity, reaching its peak at an optimal GeO$_2$ content of 50 mol%. However, higher concentrations of bismuth ions, especially exceeding 0.05 mol%, lead to the formation of detrimental Bi clusters, impairing Bi NIR luminescence. The EPR results confirms that the increased amount of Ge-ODC in the glass network is beneficial to the increase of L+ band luminescence in Bi/Ge co-doped silica glass. Notably, from the perspective of charge balance, we propose that Ge-ODC plays a pivotal role in promoting the formation of BAC-Ge and L+ band emission centered around 1680 nm. This investigation can help us to further understand the spectroscopic properties of Bi in glass and fiber.

Author contributions

Conceptualization: L. L. Hu conceived the idea. X. Li designed the experiments, performed the measurements and the

analysis, and wrote the manuscript with support from L. L. Hu; C. Y. Shao, J. M. Tian, F. Wang, Y. G. Chen, and Y. Jiao performed the measurements and analyzed the data; M. T. Guo, C. L. Yu, and L. L. Hu revised the manuscript.

Conflicts of interest

There are no conflicts to declare.

Acknowledgements

Notes and references

1 W. C. Wang, B. Zhou, S. H. Xu, Z. M. Yang and Q. Y. Zhang, *Prog. Mater. Sci.*, 2019, **101**, 90–171.
2 M. E. Fermann and I. Hartl, *Nat. Photonics*, 2013, **7**, 868–874.
3 J. K. R. Weber, J. J. Felten, B. Cho and P. C. Nordine, *Nature*, 1998, **393**, 769–771.
4 A. J. Kenyon, *Prog. Quantum Electron.*, 2002, **26**, 225–284.
5 H. Y. Fan, G. N. A. Wang, K. F. Li and L. L. Hu, *Solid State Commun.*, 2010, **150**, 1101–1103.
6 E. M. Dianov, *Light: Sci. Appl.*, 2012, **1**, 7.
7 M. Y. Peng, J. R. Qiu, D. P. Chen, X. G. Meng and C. S. Zhu, *Opt. Express*, 2005, **13**, 6892–6898.
8 M. Y. Peng, J. R. Qiu, D. P. Chen, X. G. Meng and C. S. Zhu, *Opt. Lett.*, 2005, **30**, 2433–2435.
9 X. Li, J. Cao, M. Huang and M. Peng, *J. Non-Cryst. Solids*, 2021, **553**, 120477.
10 J. Cao, S. Xu, Q. Zhang, Z. Yang and M. Peng, *Adv. Opt. Mater.*, 2018, **6**, 1801059.
11 J. Cao, L. Wondraczek, Y. Wang, L. Wang, J. Li, S. Xu and M. Peng, *ACS Photonics*, 2018, **5**, 4393–4401.
12 P. X. Xiong, Y. Y. Li and M. Y. Peng, *iScience*, 2020, **23**, 26.
13 N. K. Thipparapu, Y. Wang, S. Wang, A. A. Umnikov, P. Barua and J. K. Sahu, *Opt. Mater. Express*, 2019, **9**, 2446.
14 J. M. Tian, M. T. Guo, F. Wang, C. L. Yu, L. Zhang, M. Wang and L. L. Hu, *Chin. Opt. Lett.*, 2022, **20**, 5.
15 J. Tian, M. Guo, F. Wang, C. Wu, L. Zhang, M. Wang, Y. Wang, J. Chen, C. Yu and L. Hu, *Chin. Opt. Lett.*, 2023, **21**, 050601.
16 Y. Wang, S. Wang, A. Halder and J. Sahu, *Opt. Mater. X*, 2023, **17**, DOI: 10.1016/j.omx.2022.100219.
17 S. V. Firstov, S. V. Alyshev, K. E. Riumkin, V. F. Khopin, A. N. Guryanov, M. A. Melkumov and E. M. Dianov, *Sci. Rep.*, 2016, **6**, 6.
18 Y. Wang, N. K. Thipparapu, D. J. Richardson and J. K. Sahu, *IEEE Electron. Network*, 2021, DOI: 10.1364/OFC.2021.Tu1E.1.
19 I. A. Bufetov, M. A. Melkumov, S. V. Firstov, K. E. Riumkin, A. V. Shubin, V. F. Khopin, A. N. Guryanov and E. M. Dianov, *IEEE J. Sel. Top. Quantum Electron.*, 2014, **20**, 111–125.
20 S. Wei, M. Ding, D. Fan, Y. Luo, J. Wen and G.-D. Peng, *Bismuth – Advanced Applications and Defects Characterization*, 2018, ch. 8, DOI: 10.5772/intechopen.75106.
21 J. Šmejcký, V. Jeřábek, D. Mareš, J. Voves, P. Vařák, J. Cajzl, J. Oswald, V. Prajzler and P. Nekvindová, *Opt. Mater.*, 2023, **137**, 113621.
22 Y. Wu, J. Wen, M. Zhang, J. Wen, W. Chen, X. Zhang, F. Pang, F. Tang, G. West and T. Wang, *J. Light: Technol.*, 2022, **40**, 7922–7929.
23 P. F. Kashaykin, A. L. Tomashuk, V. F. Khopin, S. V. Firstov, A. N. Guryanov and E. M. Dianov, *J. Non-Cryst. Solids*, 2018, **496**, 24–28.
24 A. Vakhrushev, Y. Ososkov, S. Alyshev, A. Khegai, A. Umnikov, F. Afanasiev, K. Riumkin, E. Firstova, A. Guryanov, M. Melkumov and S. Firstov, *J. Light: Technol.*, 2023, **41**, 709–715.
25 G. S. Henderson, D. R. Neuville, B. Cochain and L. Cormier, *J. Non-Cryst. Solids*, 2009, **355**, 468–474.
26 A. Alessi, S. Agnello, F. M. Gelardi, G. Messina and M. Carpanese, *J. Non-Cryst. Solids*, 2011, **357**, 1900–1903.
27 L.-S. Du, L. Peng and J. F. Stebbins, *J. Non-Cryst. Solids*, 2007, **353**, 2910–2918.
28 Y. Nagayoshi, R. Matsuzaki and T. Uchino, *J. Phys. Chem. C*, 2018, **122**, 23712–23719.
29 E. M. Dianov, *Laser Phys. Lett.*, 2015, **12**, 095106.
30 V. Fuertes, F. E. Durak, V. A. G. Rivera, N. Grégoire, S. Morency, M. Sharma, L. Wang, Y. Messaddeq and S. LaRochelle, *J. Non-Cryst. Solids*, 2023, **613**, 122381.
31 S. J. Liu, H. Y. Li, Y. X. Tang and L. L. Hu, *Chin. Opt. Lett.*, 2012, **10**, 4.
32 S. Firstov, A. Kharakhordin, S. Alyshev, K. Riumkin, E. Firstova, M. Melkumov, V. Khopin, A. Guryanov and E. Dianov, *Opt. Express*, 2018, **26**, 12363–12371.
33 X. Li, M. Peng, J. Cao, Z. Yang and S. Xu, *J. Mater. Chem. C*, 2018, **6**, 7814–7821.
34 J. Cao, F. Hu, L. Chen, H. Guo, C. Duan and M. Yin, *J. Am. Ceram. Soc.*, 2017, **100**, 2108–2115.
35 S. Sun, B. Jia, B. Yan, S. Li, C. Gao, J. Wang, B. Yang and P. Lu, *J. Lumin.*, 2019, **213**, 304–309.
36 Y. Sakurai, *J. Non-Cryst. Solids*, 2006, **352**, 2917–2920.
37 N. Richard, S. Girard, L. Martin-Samos, V. Cuny, A. Boukenter, Y. Ouerdane and J. P. Meunier, *J. Non-Cryst. Solids*, 2011, **357**, 1994–1999.
38 A.-M. El-Sayed, M. Jech, D. Waldhör, A. Makarov, M. I. Vexler and S. Tyaginov, *Phys. Rev. Mater.*, 2022, **6**, 125002.
39 M. Essid, J. Albert, J. L. Brebner and K. Awazu, *J. Non-Cryst. Solids*, 1999, **246**, 39–45.
40 L. Wang, L. Tan, Y. Yue, M. Peng, J. Qiu and J. Mauro, *J. Am. Ceram. Soc.*, 2016, **99**, 2071–2076.
41 E. Culea, L. Pop and M. Bosca, *J. Alloys Compd.*, 2010, **505**, 754–757.
42 M. Ferraris, D. Milanese, C. Contardi, Q. Chen and Y. Menke, *J. Non-Cryst. Solids*, 2004, **347**, 246–253.
43 Y. Jiao, Q. Yang, M. Guo, X. Ma, C. Shao, C. Yu and A. L. Hu, *Opt. Mater. Express*, 2021, **11**, 1885.
44 M. Peng, G. Dong, L. Wondraczek, L. Zhang, N. Zhang and J. Qiu, *J. Non-Cryst. Solids*, 2011, **357**, 2241–2245.

16158 | *J. Mater. Chem. C*, 2023, **11**, 16152–16158

This journal is © The Royal Society of Chemistry 2023